Front. Electr. Electron. Eng. China 2008, 3(4): 425–434
DOI 10.1007/s11460-008-0069-4

RESEARCH ARTICLE

Ying LIU, Guisheng LIAO, Zhengguang ZHOU

Highly robust ground moving target detection and relocation method for distributed satellites

Abstract The performance of ground moving target detection for distributed satellites will be affected significantly when there is an image registration error, clutter decorrelation and array error. In this paper, a new approach to moving target detection and relocation is proposed based on multi-channel and multi-pixel adaptive signal processing in an image domain. First, multi-channel and multi-pixel joint data are equated to a simple array model. Given that there is an image registration error, the real steering vector of the moving target can be estimated through a space projection approach. The optimal beam forming approach is used to cancel clutter, and at the same time the cross-track velocity of the moving target can be determined by searching for the peak value of the cost function. The moving target can then be relocated on the SAR image. The simulation results indicate that this method has a good robustness to image registration error, clutter decorrelation and array error. The detection performance and the estimation accuracy are significantly improved.

Keywords distributed satellite, ground moving target detection, cost function, image registration error, optimal beam forming

1 Introduction

A highly sparse radar array (also called the constellation) composed of several small satellites can cooperate to perform multiple spatial missions [1–5] such as SAR imaging with a high resolution and a wide swath, ground moving target detection (GMTI) and digital elevation model (DEM). Therefore, its performance and reliability are better than those of a single conventional, larger space-borne radar.

Spaceborne SAR can carry out wide area surveillance and detect valuable military targets in time, which has a critical military significance. If receiving antennas are placed on different small satellites that run in a formation, the distance between the antennas would be longer and changeable. Consequently, the GMTI performance would be significantly improved. If only SAR imaging and GMTI are needed, the optimal satellite formation is a linear array along a track. Such an array has no resolving ability on the topography altitude to obtain optimal clutter cancellation performance.

At present, the methods for multi-channel SAR ground moving target detection mainly include displaced phase center antennas (DPCA) [6], along track interferometry (ATI) [7], and space-time adaptive processing (STAP) [8]. In the DPCA method, the velocity of the satellite, pulse repetition frequency and distance between phase centers are required to satisfy a strict condition. Thus, it is constrained in practical application. With the development of a new technique, its restriction has been relaxed step by step so that its application scope has been extended. The ATI method uses two or more phase centers placed along the track and computes their interferometric phase after time calibration to detect moving targets. The STAP method utilizes space and time information to eliminate the clutter through an adaptive processing method.

For the existing multi-channel SAR ground moving target detection methods, the GMTI performance is restricted primarily by multi-channel SAR image relativity. This relativity will degrade if there are image registration errors, especially clutter decorrelation between different channels and array error. Since the phase center positions of the synthetic aperture radars are different, there will be relative translation between SAR images. If the images are very wide and there are different geometric

Translated from *Acta Electronica Sinica*, 2007, 35(6): 1009–1014 [译自: 电子学报]

Ying LIU (✉)
National Laboratory of Radar Signal Processing, Xidian University, Xi'an 710071, China
Present address: Nanjing Research Institute of Electronics Technology, Nanjing 210013, China
E-mail: liuying1927@126.com

Guisheng LIAO, Zhengguang ZHOU
National Laboratory of Radar Signal Processing, Xidian University, Xi'an 710071, China

deformations or even rotations between images, the registration will be complicated with lower precision. To avoid collision, the baselines are tens or even hundreds of meters, the overlong along-track baseline will prevent absolute coherence of clutter from different channels. Thus, the image relativity will be reduced accordingly. In addition, array error (especially sensor position error and gain and phase error) can also cause degradation of image relativity. Therefore, research on ground moving target detection and relocation method which is highly robust to image registration error, clutter decorrelation and array error is significant. In Ref. [9] a method using the coherence information of neighboring pixels is proposed to solve the image registration problem in InSAR. In this paper, we make use of that idea and propose a new method which can jointly implement ground moving target detection and relocation based on multi-channel and multi-pixel joint adaptive processing. In this method, joint data from the multi-channel and multi-pixel approach are equated into a simple array model. Given an image registration error, the real steering vector of the moving target can be estimated through space projection. The optimal beam forming approach is used to cancel clutter, and at the same time the cross-track velocity of moving target can be determined by searching for the peak value of the cost function. The moving target can then be relocated on the image. The performance analysis and simulation results show that this method is highly robust to image registration error, and the moving target detection performance and velocity estimation accuracy are enhanced at a high degree.

The following sections are arranged as follows: In Sect. 2, we analyze the signal model of multi-channel and multi-pixel joint data. Section 3 gives the equivalent model of multi-channel and multi-pixel joint data and presents the moving target detection and relocation method. Section 4 includes performance analysis and simulation results. Finally, conclusions are provided in Sect. 5.

2 Signal model of multi-channel and multi-pixel joint data

If only SAR imaging and GMTI function are needed, the optimal satellite formant is a linear array along a track, and we thus suppose that the satellite array is a linear one along the track. Moreover, the azimuth velocity of a moving target will cause the target to defocus from the SAR image. However, the velocity of the satellite is very high and the moving target usually moves at a slow speed. Therefore, the Doppler frequency modulation rate of moving target is approximately equal to that of immobile targets, i.e., the moving target can be well focused using the Doppler frequency modulation rate of the immobile targets. For this reason, the influence of the azimuth velocity of moving target is ignored in this paper.

We first analyze the signal model of multi-channel SAR. The first satellite is regarded as the reference. After SAR imaging processing, accurate image registration and phase compensation, the signal of pixel i of the mth channel is

$$x_m(i)=c_m(i)+n_m(i),\quad m=1,\ldots,M, \tag{1}$$

where $c_m(i)$ is the clutter component of that pixel. If the incident angles of different satellites are approximately equal, the complex reflection coefficient does not change. Therefore, after accurate registration and phase compensation, the clutter component is the same for different satellites, i.e., $c_1(i)=c_2(i)=\cdots=c_M(i)=c(i)\triangleq\sigma_i$, which can be regarded as complex reflection coefficients of the pixel. $n_m(i)$ is the noise component of that pixel, and M is the number of channels.

The signals of all satellites can be written as a vector:

$$\boldsymbol{X}(i)=\boldsymbol{\alpha}c(i)+\boldsymbol{N}(i)=\begin{bmatrix}1\\ \vdots\\ 1\end{bmatrix}\sigma_i+\boldsymbol{N}(i), \tag{2}$$

where $\boldsymbol{\alpha}$ is the steering vector of clutter.

When there is image registration as shown in Fig. 1 (for convenience, the number of the satellites is supposed to be 3), then

$$\begin{aligned}\boldsymbol{X}&=\begin{bmatrix}\boldsymbol{X}_1\\ \boldsymbol{X}_2\\ \boldsymbol{X}_3\end{bmatrix}=\begin{bmatrix}\sigma_1\\ \rho_{21}\sigma_1+\rho_{22}\sigma_2\\ \rho_{31}\sigma_1+\rho_{33}\sigma_3\end{bmatrix}+\boldsymbol{N}\\ &=\begin{bmatrix}1&0&0\\ \rho_{21}&\rho_{22}&0\\ \rho_{31}&0&\rho_{33}\end{bmatrix}\begin{bmatrix}\sigma_1\\ \sigma_2\\ \sigma_3\end{bmatrix}+\boldsymbol{N}=\boldsymbol{A}\begin{bmatrix}\sigma_1\\ \sigma_2\\ \sigma_3\end{bmatrix}+\boldsymbol{N},\end{aligned} \tag{3}$$

where σ_1, σ_2, σ_3 denote the complex reflection coefficients of pixel 1, 2 and 3 respectively. ρ_{mi}, $m=2,3$, $i=1,2,3$ is the correlation coefficient of the pixel required to be detected on the mth image and the pixel i on the first image (reference image).

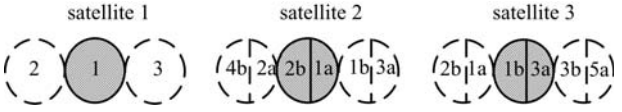

Fig. 1 Formation sketch map of pixels when there is image registration error

It can be seen from the above equation that the steering vector of the clutter cannot be simply written as $[1,\ldots,1]^{\mathrm{T}}$ and it becomes a matrix as $\boldsymbol{A}$ in Eq. (3). Furthermore, the

freedom of the clutter will increase and may be less than, equal to or even more than N. If the system controllable freedom is only N, when the freedom of the clutter is equal to or more than N, it has inadequate capability to restrain all clutters.

In such a case, full use of the clutter component information in the neighboring pixels should be made to eliminate the clutters. We can then use the pixel required to be detected and its surrounding pixels for joint adaptive processing. Given that one pixel registration precision can be obtained in coarse registration, this method can only choose the pixel that needs detecting and its adjacent pixels.

Choosing the desired pixel and its neighboring eight pixels as a rectangle, the formation sketch map of multi-channel and multi-pixel data is shown in Fig. 2. The number of satellites shown in the figure is supposed to be 3.

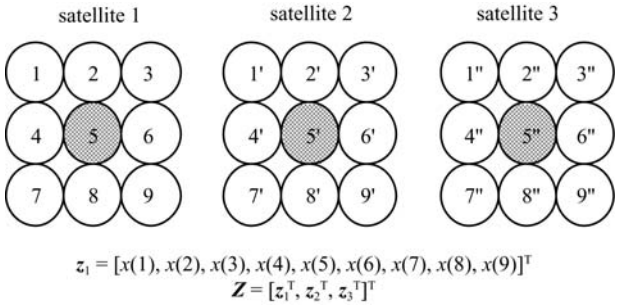

Fig. 2 Formation sketch map of multi-channel and multi-pixel data

Realign the signals as follows:

$$\boldsymbol{z}_m(i) = [x_m(i-4), x_m(i-3), \cdots, x_m(i), \cdots, x_m(i+4)]^{\mathrm{T}}, \quad m = 1, \ldots, N, \tag{4}$$

where pixel i is the one required to be detected, and $(i-4)$, …, $(i-1)$, $(i+1)$, ⋯, $(i+4)$ are its neighboring eight pixels respectively. Arrange the multi-channel signals as a vector:

$$\boldsymbol{Z}(i) = \left[\boldsymbol{z}_1^{\mathrm{T}}(i) \quad \boldsymbol{z}_2^{\mathrm{T}}(i) \quad \cdots \quad \boldsymbol{z}_N^{\mathrm{T}}(i)\right]^{\mathrm{T}}. \tag{5}$$

The dimension of this vector is $9N \times 1$. The covariance matrix of the clutter and noise can then be estimated by averaging the surrounding signals which are independently and identically distributed (i.i.d.):

$$R(i) = \frac{1}{ML} \sum_{l=-L/2}^{L/2-1} \sum_{s=-M/2}^{M/2-1} \boldsymbol{Z}(m+l, n+s) \boldsymbol{Z}^{\mathrm{H}}(m+l, n+s), \tag{6}$$

where L and M are the sample numbers along the azimuth and range respectively. To ensure the signal-to-noise ratio (SNR) loss is less than 3 dB, the condition $ML \geqslant (2 \times 9N - 1)$ should be met. In GMTI, the target signal will deteriorate the samples. To avoid that regression, some protected pixels should be reserved in estimating the covariance matrix, i.e., the pixel that needs detecting and its adjacent pixels should not be used in estimation.

3 Equivalent model of multi-channel and multi-pixel joint data and method of ground moving target detection and relocation

Build the multi-channel and multi-pixel joint adaptive processing as an array model as follows (the number of satellites is still supposed to be 3): three channels can be regarded as three sub-arrays. Each sub-array is composed of nine sensors according to nine pixels, and the signal received by each sensor is the echo of the corresponding pixel. All sensors compose a big array as shown in Fig. 3.

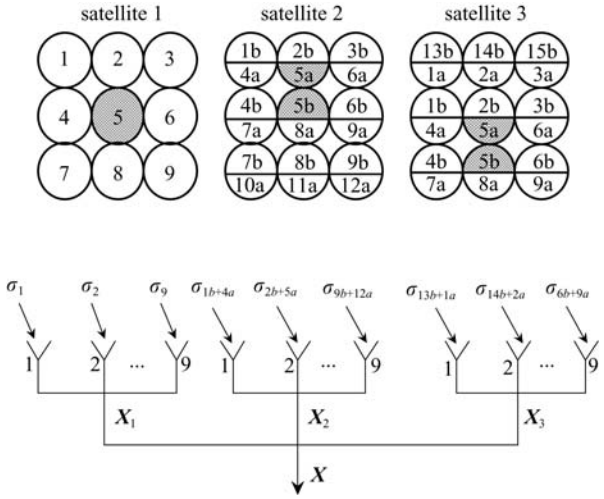

Fig. 3 Equivalent array model of multi-channel and multi-pixel joint data

Considering the moving targets, the immobile targets signals of the whole array can be expressed as

$$\boldsymbol{X} = [\boldsymbol{X}_1 \quad \boldsymbol{X}_2 \quad \boldsymbol{X}_3]^{\mathrm{T}}, \tag{7}$$

where $\boldsymbol{X}_1$, $\boldsymbol{X}_2$, $\boldsymbol{X}_3$ are signal vectors received from the three sub-arrays respectively:

$$\begin{aligned} \boldsymbol{X}_1 &= [\sigma_1, \sigma_2, \ldots, \sigma_9]^{\mathrm{T}}, \\ \boldsymbol{X}_2 &= [\sigma_{1b+4a}, \sigma_{2b+5a}, \ldots, \sigma_{9b+12a}]^{\mathrm{T}}, \\ \boldsymbol{X}_3 &= [\sigma_{13b+1a}, \sigma_{14b+2a}, \ldots, \sigma_{6b+9a}]^{\mathrm{T}}, \end{aligned} \tag{8}$$

σ_i, $i = 1, \ldots, 15$ is the complex reflection coefficient of the pixel i.

Rewrite Eq. (7) in the following form:

$$\boldsymbol{X} = \boldsymbol{A}\boldsymbol{C} + \boldsymbol{N}, \tag{9}$$

where $\boldsymbol{A}$ is the manifold of the array, and every column of

$\boldsymbol{A}$ denotes the steering vector of one signal. From the independence of the clutter it can be known that $\boldsymbol{C}=[\sigma_1,\sigma_2,\ldots,\sigma_9,\sigma_{10},\sigma_{11},\sigma_{12},\sigma_{13},\sigma_{14},\sigma_{15}]^{\mathrm{T}}$. The number of the source in $\boldsymbol{C}$ is the clutter freedom. $\boldsymbol{N}$ is the noise vector received by the array.

The steering vector form of the signal will be analyzed in detail as follows. Define the steering vector of the signal according to pixel i under an array model as

$$\boldsymbol{S}_i=\boldsymbol{S}_{si}\circ\boldsymbol{S}_{pi}, \tag{10}$$

where "$\circ$" denotes the Hadamand product. $\boldsymbol{S}_{si}$ is the spatial steering vector of the signal. For the clutter on the ground, the spatial steering vector is $\boldsymbol{S}_{si}=[1,1,1]^{\mathrm{T}}$. $\boldsymbol{S}_{pi}$ is the correlation coefficient vector of the signal. Let $\boldsymbol{S}_{pi}=[\boldsymbol{S}_{pi1},\boldsymbol{S}_{pi1},\boldsymbol{S}_{pi3}]^{\mathrm{T}}$, where $\boldsymbol{S}_{pi1}$, $\boldsymbol{S}_{pi2}$, $\boldsymbol{S}_{pi3}$ are correlation coefficient vectors on the three sub-arrays respectively. When the images are registered accurately, $\boldsymbol{S}_{pi1}$, $\boldsymbol{S}_{pi2}$, $\boldsymbol{S}_{pi3}$ are equal to the ith column of the unit matrix $\boldsymbol{I}_{9\times 9}$. In this case, only one of the three elements of the correlation coefficient vector is one and the others are zeros. For convenience, we define this correlation coefficient vector as the "perfect correlation coefficient vector" and the corresponding steering vector as the "perfect steering vector". However, when image registration error exists, a part of or almost the whole pixel i moves out of its position, and the correlation coefficient vector of this pixel is no longer perfect. Only several elements of this correlation coefficient vector are nonzero, while the number of the nonzero elements may not be 3 and the value of these elements is definitely not 1. The nonzero element denotes that it contains a component of the pixel i. In this case, the real steering vector of the pixel is required to be estimated based on the real image registration error.

Suppose the moving target is in pixel 5. Therefore, the perturbance of the moving target's correlation coefficient vector caused by image registration error is the same as that of pixel 5.

First, compute the correlation coefficients of the pixel that are required to be detected on the nth image ($n=2,3,\ldots,M$) with the required to be detected pixel and its adjacent eight pixels on the first image. The image registration error direction of the nth image from the reference image can be determined by comparing magnitudes of the correlation coefficients. The positions of nonzero elements in the correlation coefficient vector on the sub-array according to that image then can be determined. For example, the image registration error direction of the second image is shown in Fig. 1. Since part of pixel 5 moves into pixel 2, the correlation coefficient of the pixel required to be detected with its upper pixel is much bigger than those with the other adjacent pixels. We simulated the condition that the image registration error is up 0.4 pixel. The correlation coefficients of the required to be detected pixel on the second image with the nine pixels on the first image are 0.0451, 0.5064, 0.0455, 0.0526, 0.7585, 0.0368, 0.0128, 0.0970, 0.0483, respectively.

After determining the positions of nonzero elements in the correlation coefficient vector of pixel 5, suppose the initialization of its correlation coefficient vector formation is

$$\begin{aligned}\boldsymbol{S}_{p5}^0&=\left[\boldsymbol{S}_{p51}^0,\boldsymbol{S}_{p52}^0,\boldsymbol{S}_{p53}^0\right]^{\mathrm{T}}\\&=\Big[\underbrace{0,\cdots,0}_{4},1,\underbrace{0,\cdots,0}_{4},0,1,0,0,1,\underbrace{0,\cdots,0}_{4},\\&\quad\underbrace{0,\cdots,0}_{4},1,0,0,1,0\Big]^{\mathrm{T}}_{27\times 1}.\end{aligned} \tag{11}$$

The result of Eq. (11) is gained based on the image registration error shown in Fig. 3. From Eq. (10), the initial steering vector of pixel 5 can be written as

$$\begin{aligned}\boldsymbol{S}_5^0&=\boldsymbol{S}_{s5}\circ\boldsymbol{S}_{p5}^0=[1,1,1]^{\mathrm{T}}\circ\left[\boldsymbol{S}_{p51}^0,\boldsymbol{S}_{p52}^0,\boldsymbol{S}_{p53}^0\right]^{\mathrm{T}}\\&=\Big[\underbrace{0,\cdots,0}_{4},1,\underbrace{0,\cdots,0}_{4},0,1,0,0,1,\underbrace{0,\cdots,0}_{4},\\&\quad\underbrace{0,\cdots,0}_{4},1,0,0,1,0\Big].\end{aligned} \tag{12}$$

This steering vector is the same as the real one only in form and the values of its elements have errors. We make use of the space projection method [10] to resolve such problem. The more important step is to determine their values.

By performing eigenvalue decomposition on the covariance matrix of clutter and noise expressed in Eq. (6):

$$\boldsymbol{R}\overset{\mathrm{EVD}}{=}\boldsymbol{U}_c\boldsymbol{\Lambda}_c\boldsymbol{U}_c^{\mathrm{H}}+\boldsymbol{U}_M\boldsymbol{\Lambda}_M\boldsymbol{U}_M^{\mathrm{H}}, \tag{13}$$

where $\boldsymbol{U}_c$ and $\boldsymbol{U}_M$ are composed of eigen-vectors according to P large eigenvalues and $M-P$ small eigenvalues respectively. $\boldsymbol{\Lambda}_c$ is a diagonal matrix and its diagonal elements are P large eigenvalues in descending order. The diagonal elements of $\boldsymbol{\Lambda}_N$ are $M-P$ small eigenvalues which are approximately equal. The column space of $\boldsymbol{U}_c$, which is expressed as span($\boldsymbol{U}_c$), is the clutter sub-space of the received signal. The projective matrix on the clutter sub-space is

$$\boldsymbol{P}_c\overset{\mathrm{def}}{=}\boldsymbol{U}_c\left(\boldsymbol{U}_c^{\mathrm{H}}\boldsymbol{U}_c\right)^{-1}\boldsymbol{U}_c^{\mathrm{H}}=\boldsymbol{U}_c\boldsymbol{U}_c^{\mathrm{H}}. \tag{14}$$

For the real steering vector, pixel 5 is included in clutter sub-space, and the real steering vector and the real correlation coefficient vector of pixel 5 can be obtained by projecting Eq. (12) on the clutter sub-space:

$$\boldsymbol{S}_5=\boldsymbol{S}_{s5}\circ\boldsymbol{S}_{p5}=\boldsymbol{P}_c\boldsymbol{S}_5^0=\boldsymbol{U}_c\boldsymbol{U}_c^{\mathrm{H}}\boldsymbol{S}_5^0. \tag{15}$$

For the moving target, the correlation coefficient vector is the same as that of the clutter in the pixel where the

moving target lies. However, the spatial steering vector of the moving target is different because of its cross-track velocity, and its spatial steering vector can be expressed as

$$\gamma(v_r)=\left[1,\exp\left(-\mathrm{j}\frac{4\pi v_r d_2}{\lambda v_a}\right),\exp\left(-\mathrm{j}\frac{4\pi v_r d_3}{\lambda v_a}\right)\right]^{\mathrm{T}}, \quad (16)$$

where d_n, $n=2,3$ denotes distance from the equivalent phase center of the nth satellite to the reference satellite along the track. v_a is satellite velocity, v_r is cross-track velocity of the moving target and λ is the wavelength. The real steering vector of moving target can then be obtained

$$\begin{aligned}\boldsymbol{\eta}(v_r)&=\gamma(v_r)\circ\boldsymbol{S}_{p5}\\&=\left[1,\exp\left(-\mathrm{j}\frac{4\pi v_r d_2}{\lambda v_a}\right),\exp\left(-\mathrm{j}\frac{4\pi v_r d_3}{\lambda v_a}\right)\right]^{\mathrm{T}}\\&\quad\circ\left[\boldsymbol{S}_{p51},\boldsymbol{S}_{p52},\boldsymbol{S}_{p53}\right]^{\mathrm{T}}.\end{aligned} \quad (17)$$

When the beam forms on the signal using the weight vector composed of the real steering vector of the moving target, the moving target signal is coherently accumulated and its output is maximal. However, the steering vector of the clutter is different from that of the moving target so that its output is less. Using the linear constraint minimal variance criterion [11], the adaptive weight vector can be constructed as

$$\boldsymbol{w}(v_r)=\mu\boldsymbol{R}^{-1}\boldsymbol{\eta}(v_r), \quad (18)$$

where μ is a complex constant.

Use the adaptive weight expressed in Eq. (18) for multi-channel and multi-pixel joint adaptive beam formation on the pixel where the target lies. When v_r in the constructed adaptive weight is equal to the moving target cross-track velocity, the output signal to clutter and noise ratio is maximal. Thus, we construct a cost function as follows:

$$\begin{aligned}J(v_r)&=\frac{E_{S_{\mathrm{out}}}}{(E_C+E_M)_{\mathrm{out}}}\frac{(E_C+E_M)_{\mathrm{in}}}{E_{S_{\mathrm{in}}}}\\&=\frac{E_{S_{\mathrm{out}}}}{(E_C+E_M)_{\mathrm{out}}}\frac{(\mathrm{CNR}+1)\sigma_n^2}{E_{S_{\mathrm{in}}}},\end{aligned} \quad (19)$$

where $E_{S_{\mathrm{in}}}$ and $E_{S_{\mathrm{out}}}$ are input and output average power of the signal respectively. $(E_C+E_M)_{\mathrm{in}}$ and $(E_C+E_M)_{\mathrm{out}}$ are input and output average power of the clutter and noise. CNR is the average clutter to noise ratio in the image domain, while σ_n^2 is the input average power of noise. The cost function denotes the ratio of output signal to clutter and noise ratio ($\mathrm{SCNR}_{\mathrm{out}}$) to input signal to clutter and noise ratio ($\mathrm{SCNR}_{\mathrm{in}}$). It can weigh the degree of SCNR improvement. Change v_r to find the maximum of the cost function so that cross-track velocity estimation $\bar{v}_r$ of the moving target can be obtained. It should be mentioned that the cost function is very important when estimating the cross-track velocity of the moving target. The clutter has randomness, which may induce the output average power of the clutter to be larger than that of the signal. For that reason, the cost function cannot be constructed as the power spectrum in the conventional Capon approach, i.e., the performance of weight can not be evaluated by finding the maximum of the output power, but by finding the maximum output signal ratio to clutter and noise ratio to input signal to clutter and noise ratio. The clutter power here means the average clutter and noise power of the whole range cell.

A search can only be performed in the pixel where the target lies so that the computational complexity is very minimal. In the search process, along track distances between satellites are supposed to be accurate. When there are errors in satellite positions, the velocity estimation error will exist accordingly. The detailed analysis is given in Sect. 4.

After the cross-track velocity estimation is gained, the real azimuth position of target can be solved by the following equation and then the target can be relocated on the SAR image:

$$\bar{x}=x_0+\bar{v}_r\frac{r(i)}{v_a}, \quad (20)$$

where x_0 is the false azimuth position of target on the SAR image and $r(i)$ is the slant range from the satellite to the target in the middle of illuminating time.

The presence of blind speed is the most important question in the cross-track velocity estimation process. It can be seen from the spatial steering vector expressed in Eq. (16) that blind speed will exist when the phase is equal to integer times 2π. Since multi-channel processing is used in this paper, when the distances between satellites are uneven, the velocity scope where there is no blind speed can be extended. Because if and only if the equation set below is satisfied, the blind speed will exist.

$$\begin{cases}\dfrac{2v_r d_2}{\lambda v_a}=k, & k \text{ is integer},\\ \cdots & \\ \dfrac{2v_r d_M}{\lambda v_a}=l, & l \text{ is integer}.\end{cases} \quad (21)$$

When the least common multiple of $d_2,\ldots,d_M$ is very large, a wider velocity scope without blind speed can be obtained. When the number of satellites is small, for example, when there are three satellites, the system controllable freedom is very limited so that the speed response is not very good outside the slow speed region. But it can satisfy our requirement of detecting the slow targets. However, an increase of the satellites will enhance the speed response, although the cost and computational complexity will be increased accordingly. In this paper, the emphasis is put on the moving target detection method which can be done with the least number of satellites and minimal computational complexity.

But the problem is that the above method is based on the supposition that the moving target position is already known on the SAR image. In practice, the position of the moving target on the SAR image is not defined, thus performing the above processing on the whole SAR image is impractical. Hence, the moving target position on the SAR image should be determined first.

Because the spatial steering vector and correlation coefficient vector of the moving target is unknown before detection, it can be replaced by $\boldsymbol{\beta} = [1,0,\ldots,0]^{\mathrm{T}}$ to minimize the clutter output power, but cannot ensure that the target signal has no loss. The weight vector used to eliminate the clutter then becomes

$$\boldsymbol{w} = \mu \boldsymbol{R}^{-1} \boldsymbol{\beta}. \tag{22}$$

Adaptive beam forming is done on every pixel on the SAR image using the above weight vector. The moving targets can be detected by constant false alarming ratio (CFAR). The structured diagram of the proposed method is given in Fig. 4.

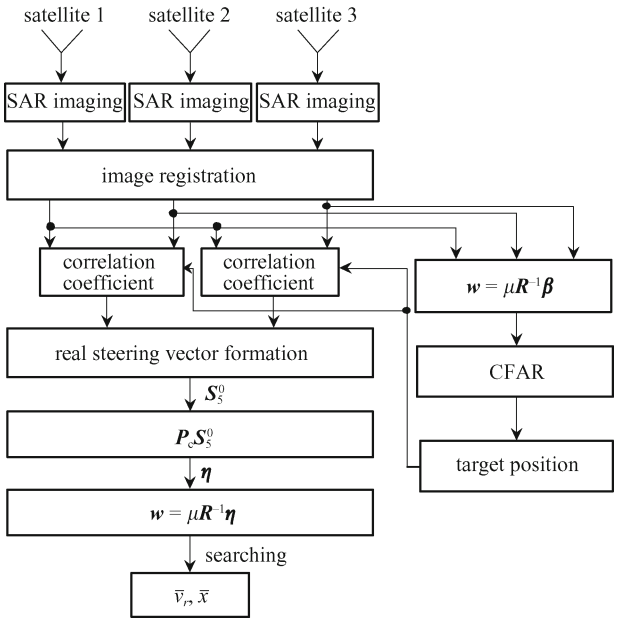

Fig. 4 Structured diagram of proposed method

4 Performance analysis and simulations

The proposed method has been verified with several simulated results and its performance has been analyzed. The parameters used in simulations are as follows. The satellite array is composed of three satellites, whose along track position is 0, 133, 217 m. The satellite velocity is $v = 7000$ m/s, and their height from the ground is $h = 800$ km. The observing range is $R = 1000$ km. The radars work at $\boldsymbol{X}$ band and the wavelength is $\lambda = 0.03$ m. The pulse repetition frequency is $f_{\mathrm{r}} = 1400$ Hz. Some airborne real data is used in the simulations. We obtained the complex reflection coefficients of the scene from the real data and simulated echo data of the three satellites using the coefficients. The height of the simulated ground scene is plain. A moving target which has only cross-track velocity was put on the scene, CNR = 30 dB, SCR = 0 dB. The required to be detected pixel and its adjacent pixels were avoided when estimating the covariance matrix.

4.1 Performance of ground moving target detection

In the analysis above, for the conventional DPCA and ATI moving target detection methods, the precision of image registration will affect the clutter cancellation performance directly. However, the proposed method in this paper has a good robustness to image registration error because it coherently and jointly uses multi-channel and multi-pixel to do adaptive processing. Figure 5 shows the performance comparisons of conventional DPCA and this method at three conditions.

From Fig. 5 we can see that when the registration error is a bit large such as 0.2 pixel or more, the conventional DPCA method cannot detect the target while the method proposed in this paper can do it well.

Besides the image registration error, the clutter correlation performance will affect the clutter cancellation performance. Fortunately, the proposed method in this paper makes use of multi-channel and multi-pixel joint adaptive processing; therefore, the influence of clutter decorrelation on detection performance is significantly reduced. In the simulation, the first satellite is considered as the reference, while each of the other two satellites is added on a random fluctuation. The amplitude satisfies a Gaussian distribution with a mean of zero and a variance of 0.1, while the phase satisfies uniform distribution between 0–0.2π. The variation curve of improvement factor (IF) gained with DPCA and the method proposed in this paper with clutter correlation coefficient is shown in Fig. 6. The definitions of the improvement factor and the correlation coefficient are

$$\mathrm{IF(dB)} = \frac{\mathrm{SCNR_{out}}}{\mathrm{SCNR_{in}}}, \tag{23}$$

$$\rho = \frac{\left| \sum_{k=-K}^{K} \sum_{s=-S}^{S} x_1(i+k,j+s) x_2^*(i+k,j+s) \right|}{\sqrt{\sum_{k=-K}^{K} \sum_{s=-S}^{S} x_1(i+k,j+s) x_1^*(i+k,j+s) \sum_{k=-K}^{K} \sum_{s=-S}^{S} x_2(i+k,j+s) x_2^*(i+k,j+s)}}, \tag{24}$$

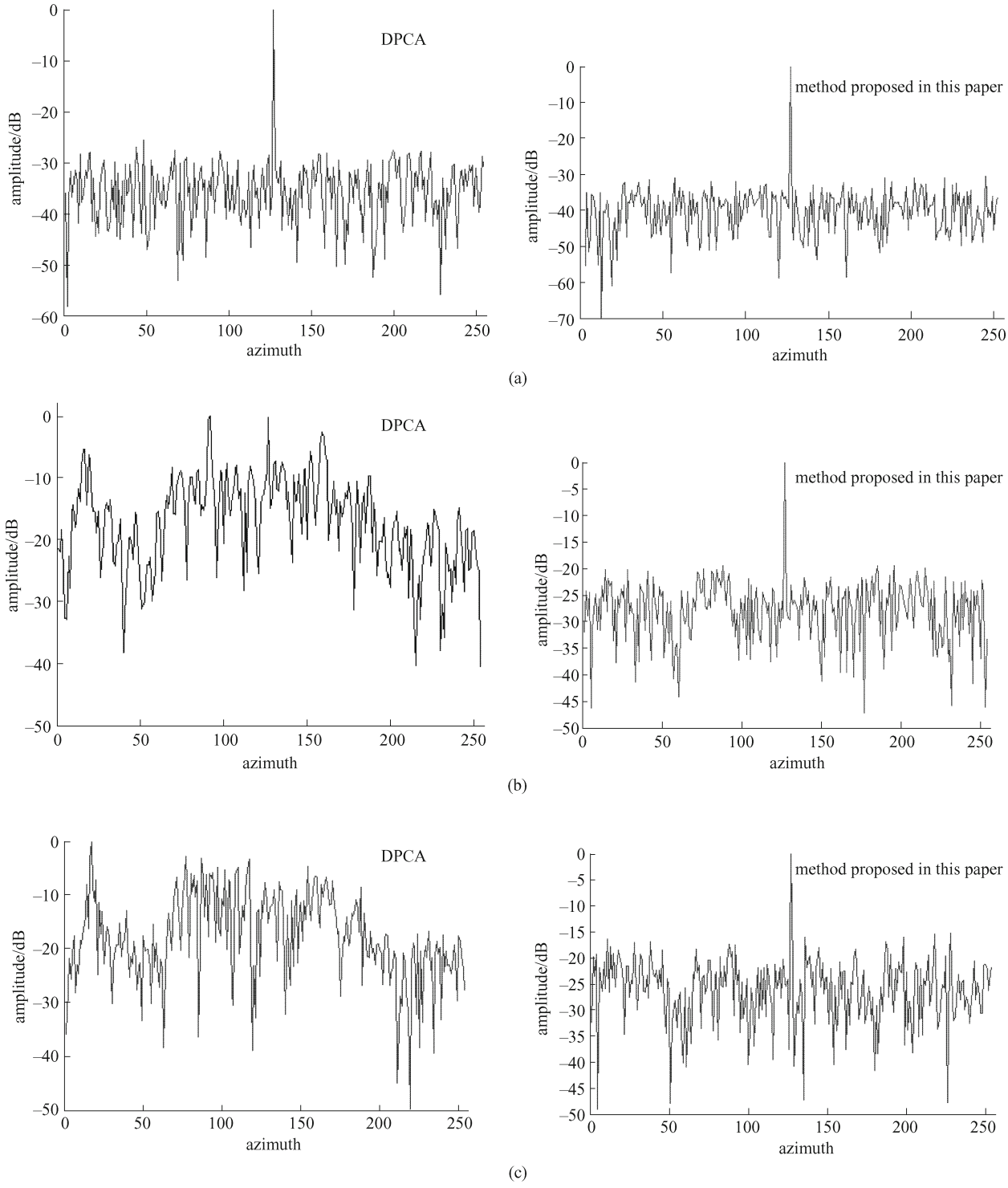

Fig. 5 Comparison of DPCA and method proposed in this paper. (a) Accurate registration; (b) registration error is (0, left 0.25, down 0.5) pixels; (c) registration error is (0, left 0.75, down 1.5) pixels

where x_1, x_2 denote the signals of the corresponding pixels on two SAR images respectively. The correlation is calculated by averaging the $(2K+1)(2S+1)$ surrounding pixels around the required computed pixel.

It can be seen from the figure that when the clutter correlation is dropped to 0.97, the IF gained with this method is still more than 24 dB. However, the performance of DPCA is much poorer.

For the conventional GMTI methods, the array error has a severe effect on GMTI performance. The inter-channel inconsistency would lead to a remainder after clutter cancellation. For the side-looking distributed SAR with

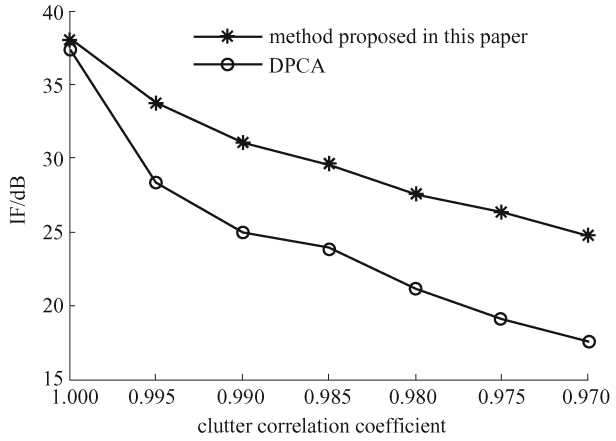

Fig. 6 Improvement factor VS clutter correlation coefficient

narrow azimuth beam, the cross-track position error can be equivalent to the inter-channel gain and phase error. Fortunately, the proposed method in this paper has a good error suppression ability of gain and phase error caused by the two above reason. Figure 7 shows the simulation results when there is a gain and phase error. We can see that this method can obtain a good performance when there is a 10% gain and phase error and cross-track position error in decimeters.

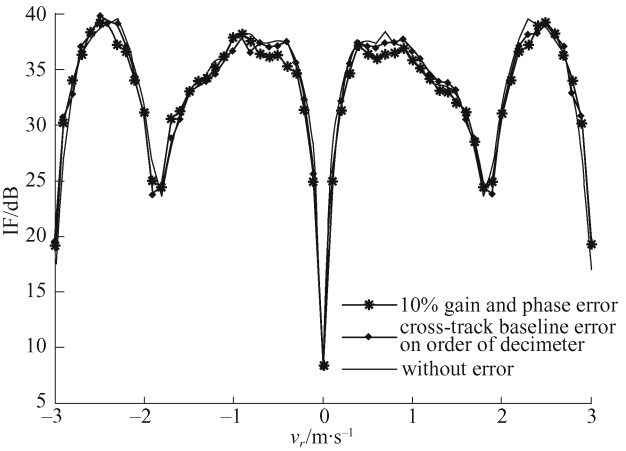

Fig. 7 GMTI performance with array error

4.2 Performance of cross-track velocity estimation and relocation of moving target

Given that the real steering vector of the moving target can be estimated through the space projection approach when there is an image registration error and the optimal beam forming approach using the real steering vector formation is performed to search for the peak of cost function, a higher accuracy of velocity estimation can be obtained. The left figures of Figs. 8(a)–8(d) show results with statistics of the cross-track velocity estimation error under four conditions.

The estimation results are obtained statistically 1200 times. In every estimation process the cross-track velocity of the moving target is randomly distributed in [0,5] m/s.

The estimation results by the two methods are shown in Fig. 8. One method estimates velocity using the real steering vector estimated by the method proposed in this paper, while another estimates velocity using the perfect steering vector defined above. It can be seen from the comparison of these two methods that the accuracy of the method in this paper is much higher and that most estimation results are less than 0.08 m/s. The results around 1 m/s are speed ambiguities caused as a result of the velocity near the high side-lobe in speed response. If the velocity is estimated with the perfect steering vector form without estimating the real steering vector, the estimation error is much larger, especially for a larger image registration error. For example, if the image registration error is about 1 pixel, this method will be a complete failure. However, the method proposed in this paper can still obtain satisfying results even under the condition that image registration error is along the tilted direction (the condition of Fig. 8(d)). Therefore, this method is applied to arbitrary direction of the image registration error. The right figures of Figs. 8(a)–8(d) give the results with statistics of relocation errors based on the velocity estimation results shown in the left ones.

After imaging and registration, the along-track position error can be compensated so that it has no influence on the moving target detection. However, accurate along-track baselines are needed in velocity estimation and relocation. When along-track baselines have errors, a velocity estimation error will be generated and then relocation cannot be done accurately. The velocity estimation result is shown in Fig. 9 under the condition that there are along-track baseline errors in decimeters. Although the estimation error exists, it is tolerable because the target velocity is very low and the baseline errors are only in decimeters.

5 Conclusions

Spaceborne GMTI can carry out wide area surveillance from a high altitude, which has critical value in military applications. However, when the image registration error, clutter decorrelation and array error exist, the GMTI performance of conventional DPCA and ATI methods would be significantly affected, such as increasing false alarm probability and even resulting in complete failure. Therefore, we researched on the GMTI method which has robustness to image registration error, clutter decorrelation and array error. A new method which can jointly implement ground moving target detection and relocation is proposed in this paper based on multi-channel and multi-pixel adaptive signal processing in an image domain. In this method, the joint data from the

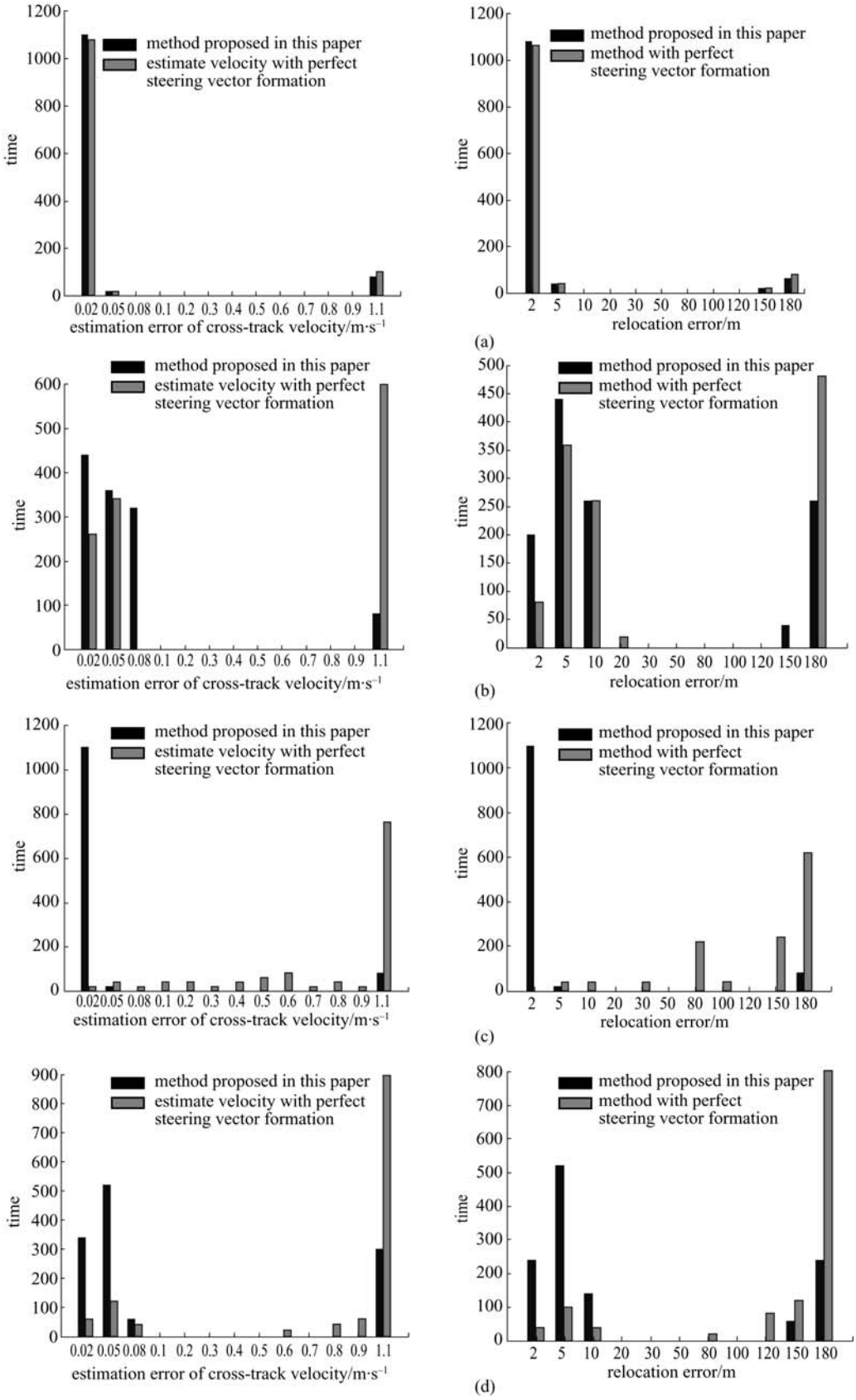

Fig. 8 Cross-track velocity estimation and relocation results of moving target. (a) Accurate registration; (b) registration error is (0, right 0.2, up 0.5) pixels; (c) registration error is (0, 0, up 1.0) pixels; (d) registration error is (0, left 0.5 × down 0.5, up 0.5) pixels

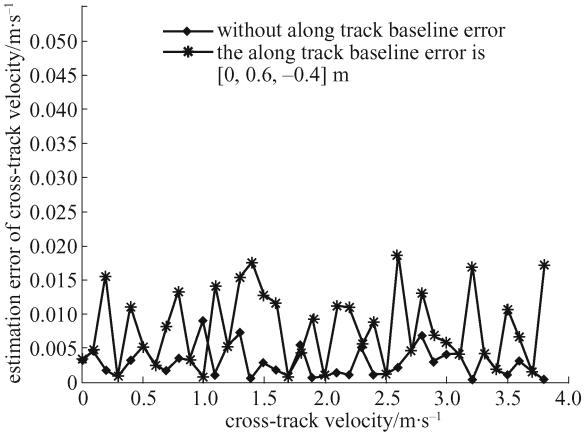

Fig. 9 Velocity estimation result with along-track baseline error

multi-channel and multi-pixel are equated to/expressed in a simple array model and the real steering vector of the moving target under the condition that the image registration error can be estimated through a space projection approach. The optimal beam forming approach is used to cancel clutter. At the same time, the cross-track velocity of the moving target can be determined by searching for the peak value of the cost function and the moving target can then be relocated on the image. Because moving target detection and velocity estimation can be done without increasing satellite number and computational complexity, this method has practical significance. The performance analysis and simulation results show that this method has a good robustness to image registration error, and the moving target detection performance and velocity estimation accuracy are improved.

Acknowledgements This work was supported by the National Natural Science Foundation of China (Grant No. 60472097).

References

1. Massonnet D. The interferometric cartwheel: a constellation of passive satellites to produce radar images to be coherently combined. International Journal of Remote Sensing, 2001, 22(12): 2413–2430
2. Goodman N A, Lin S C, Rajakrishna D, et al. Processing of multiple-receiver spaceborne arrays for wide-area SAR. IEEE Transactions on Geoscience and Remote Sensing, 2002, 40(4): 841–852
3. Luu K, Martin M, Stallard M, et al. University nanosatellite distributed satellite capabilities to support TechSat21. In: Proceedings of the 13th AIAA/USU Conference on Small Satellites (SSC99-III-3), USA. 1999, 1–9
4. Das A, Cobb R, Stallard M. TechSat21: a revolutionary concept in distributed space based sensing. In: Proceedings of AIAA Defense and Civil Space Programs Conference Exhibit, Huntsville. 1998, 896–901
5. Ramongassie S, Phalippou L, Thouvenot E, et al. Preliminary design of the payload for the interferometric cartwheel. In: Proceedings of IEEE 2000 International Geoscience and Remote Sensing Symposium. 2000. 3: 1004–1006
6. Wang H S C. Mainlobe clutter cancellation by DPCA for space-based radars. IEEE Aerospace Applications Conference. New York Piscataway: IEEE Press, 1991, 1–128
7. Frasier S J, Camps A J. Dual-beam interferometry for ocean surface current vector mapping. IEEE Transactions on Geoscience and Remote Sensing, 2001, 39(2): 401–414
8. Klemm R. Introduction to space-time adaptive processing. Electronics & Communication Engineering Journal, 1999, 11(1): 5–12
9. Li Zhenfang, Bao Zheng, Li Hai, et al. Image autocoregistration and InSAR interferogram estimation using joint subspace projection. IEEE Transactions on Geoscience and Remote Sensing, 2006, 44(2): 288–297
10. Feldman D, Griffiths L J. A projection approach for robust adaptive beamforming. IEEE Transactions on Signal Processing, 1994, 42(4): 867–876
11. Frost O L III. An algorithm for linearly constrained adaptive array processing. In: Proceedings of the IEEE. 1972, 60(8): 926–935